Applications of Electromagnetic Phenomena in Electrical and Mechanical Systems
S.Yamada, A.Nafalski and S.C. Mukhopadhyay (eds.)

Derivation from current density distribution to conductivities based on the adjoint field theory and numerical test with finite volume method*

Guoya Dong[1, 2], Xinshan Ma[1], Shangkai Gao[1], Yaoqin Xie[1], Yoshifuru Saito[3]
([1]*Department of Electrical Engineering, Tsinghua University, Beijing, 100084, CHINA, Tel:(8610) 62785472*
[2] *Hebei University of Technology, Tianjin, 300130, China*
[3] *Department of Information, Electronics and Electrical Engineering, Hosei University, 3-7-2 Kajino, Koganei, Tokyo 184-8584, JAPAN*)
dgy99@mails.tsinghua.edu.cn

ABSTRACT: To calculate the conductivities from current density distribution in the bounded region, we have previously proposed a new method based on the adjoint field theory. In this paper, we apply this new method to inhomgenous media along with the Finite Volume Method (FVM). As a result, we have succeeded in obtaining the absolute conductivity values with high accuracy.

1 INTRODUCTION

Conductivity distribution of the head tissues is of paramount importance to realize for high-resolution electroencephalography (EEG). Principal purpose of the Electrical Impedance Tomography (EIT) is to obtain the internal conductivity distribution of a bounded region by measuring the surface voltages when injecting the currents into the target region. Because of its portability and cheapness, EIT is being developed for not only non-invasive measurement to obtain the conductivities distribution of head tissues but also for brain function research. However, skull having low conductivity makes major of the injected current shunted through the scalp having high conductivity. This is a limitation of the brain research employing EIT. Due to the practical measurement accuracy, it has been possible to reconstruct the coarse conductivity distribution images by EIT.

In recent ten years, magnetic resonance imaging (MRI) makes it possible to measure the current density distribution in a simple human head phantom [1]. Consideration of this MRI technology has led us to propose a new methodology based on the adjoint field theory to calculate the absolute values of conductivities in the bounded region [2]. To verify our methodology based on adjoint field theory, 2D circular as well as 3D spherical regions consisting of homogenous media have been intensively examined in an analytical manner [3].

In this paper, we apply our method based on the adjoint field theory to the 2D circular and 3D spherical regions having inhomogeneous conductivity distribution. To verify its validity in numerically, it is essential to solve the EIT forward problem. We employ the Finite Volume Method (FVM) to solve the forward problem instead of the other commonly used numerical methods, e.g. FDM, FEM and BEM. FVM is one of the numerical methodologies in computational fluid dynamic problems. In 1994, FVM was first introduced to solve for the

* Project 59937160 supported by NSFC.
Project 501037 supported by HBNSF.

volume conductor equation in bioelectrical studies of a concentric spherical model of human head for investigating the influence of skull thickness on the scalp potential distribution [4-6]. After that, FVM has been applied to solve a large variety of bioelectric problems, i.e., the electrical activity of the heart in the torso or fetus heart in the abdomen, electrical activity in human head model. Since current continuity condition should be rigorously satisfied in current fields, then we employ FVM for solving EIT forward problem.

2 CONDUCTIVITY DERIVIATION BASED ON THE ADJOINT FIELD THEORY

In this chapter, we derive a conductivity evaluation method based on the adjoint field theory from known current densities. At first, we introduce the adjoint fields by the way of EIT example. As shown in Fig.1 (a), injecting a current I into a circular region Ω through a driving electrode pair A-B generates an original electric current field while the electric potentials at a measurement electrode pair C-D could be measured. Both of the driving and measurement electrode pairs are located at the surface Γ of the target region Ω. Conversely, injecting a current I into the same circular region Ω through a measurement electrode pair C-D generates an adjoint electric current field corresponding to the original one while the electric potentials at the driving electrode pair A-B could be measured.

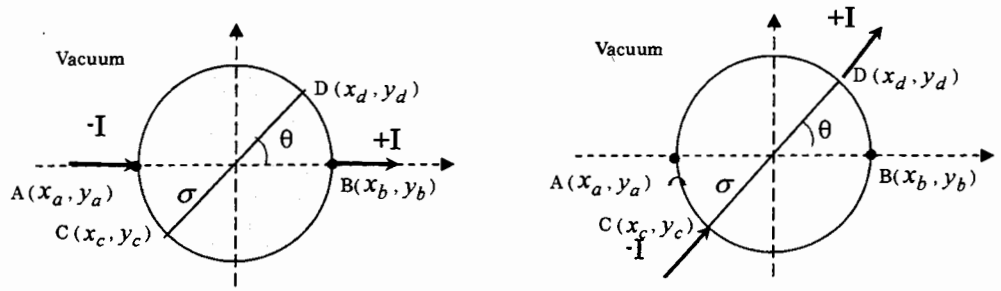

Fig. 1. Illustration of the (a) original and (b) adjoint fields.

In static electric fields, by considering the divergence theorem in an arbitrary closed bounded region Ω whose boundary is a piecewise smooth surface, we have Eqs.(1) and (2).

$$\oiint_{\Gamma} (\varphi_1 \mathbf{D}_2)_n \, d\Gamma = \iiint_{\Omega} \nabla \bullet (\varphi_1 \mathbf{D}_2) \, d\Omega = -\iiint_{\Omega} \mathbf{E}_1 \bullet \mathbf{D}_2 \, d\Omega + \iiint_{\Omega} \varphi_1 \rho_2 \, d\Omega \qquad (1)$$

$$\iiint_{\Omega} \mathbf{E}_1 \bullet \mathbf{D}_2 \, d\Omega = -\oiint_{\Gamma} (\varphi_1 \mathbf{D}_2)_n \, d\Gamma + \iiint_{\Omega} \varphi_1 \rho_2 \, d\Omega \qquad (2)$$

where the subscripts 1 and 2 refer to the original and adjoint field, respectively. $\mathbf{E}_1, \varphi_1$, $\mathbf{D}_2$, ρ_2, n are the original electric field, original potential, adjoint displacement, adjoint charge density, outward facing normal component, respectively.

Since an analogy between the static electric and current fields as well as the relationships $\rho_2 = 0$ and $\mathbf{E}_1 = \mathbf{J}_1/\sigma$ is held, then substituting an adjoint current density $\mathbf{J}_2$ for the term $\mathbf{D}_2$ in Eq.(2) yields [3]

$$\iiint_{\Omega} \frac{\mathbf{J}_1 \bullet \mathbf{J}_2}{\sigma} d\Omega = (\varphi_{1C} - \varphi_{1D}) \cdot I, \tag{3}$$

where $\sigma, \mathbf{J}_1, \mathbf{J}_2, \varphi_{1C}$ and φ_{1D} are the conductivity distribution in the target region Ω, original, adjoint current densities, the original potentials at the electrodes C and D, respectively.

Thus, if the original $\mathbf{J}_1$ and adjoint $\mathbf{J}_2$ can be measured, then it is possible to evaluate the conductivity σ by Eq.(3). This is our conductivity evaluation methodology based on the adjoint field theory.

3 NUMERICAL VERIFICATION OF METHODOLOGY BASED ON THE ADJOINT THEORY

To verify our methodology to a target region consisting of the inhomogeneous conductivity, it is essential to obtain the original $\mathbf{J}_1$ and adjoint $\mathbf{J}_2$ in Eq.(3). In practical human brain, MRI may be available to evaluate the current densities $\mathbf{J}_1$ and $\mathbf{J}_2$. In this paper, we employ the FVM instead of MRI to evaluate the current densities $\mathbf{J}_1$ and $\mathbf{J}_2$. Thus, the application of FVM on the EIT forward problem is firstly introduced below in detail.

3.1 FVM for EIT forward problem

Key idea of FVM is based on the current flow conservation law, which corresponds to the KCL equation in the electric circuits, i.e., the distribution of the potentials in the presence of current sources in a control volume V with the face S is given by the Gauss law,

$$\oiint_{S} (-\sigma \nabla \varphi) \cdot d\vec{S} = \iiint_{V} I_v dV \tag{4}$$

where σ, φ, I_v are the conductivity, potential and volume current source density in the control volume, respectively. In EIT, there is no current volume source I_v in the bounded region. Thereby, Eq.(4) reduces into

$$\oiint_{S} (-\sigma \nabla \varphi) \cdot d\vec{S} = 0. \tag{5}$$

The boundary conditions are as follows

$$\begin{cases} -\sigma \dfrac{\partial \varphi}{\partial n} = J_n & \text{at the points with current injected through the boundary } \Gamma \\ \sigma \dfrac{\partial \varphi}{\partial n} = 0 & \text{the other points of } \Gamma \end{cases},$$

where J_n is the outward facing normal component of the current density distribution.

The target region is subdivided into a large number of triangular elements in 2D and the tetrahedral elements in 3D, respectively. These elements are called the primary cells in FVM. Besides the primary cells, enclosing each of the nodes, the complementally cell is constructed to calculate the current flow across each integration face.

Fig.2 illustrates the primary and complementally cells. In 2D, a node O is common to 6 triangular elements as shown in Fig.2 (a), and also M_{ai}, M_{bi}, i =1,2…6, are the middle points of the triangle edges enclosing the common node O. Connecting these middle points, M_{ai}, M_{bi}, i =1,2…6, leads to the complementally cell enclosing the node O shown by the shadowed

region in Fig.2(a). In each of the complementally cells, Eq.(5) reduces into a following discretized form as

$$\oint\!\!\!\oint_{i^{th}} (-\sigma \nabla \varphi) \cdot d\bar{l}_i = 0, \tag{6}$$

where i refers to the i^{th} node in the primary as well as the i^{th} complementally cells, and l_i is the boundary of the i^{th} complementally cell enclosing the common i^{th} node.

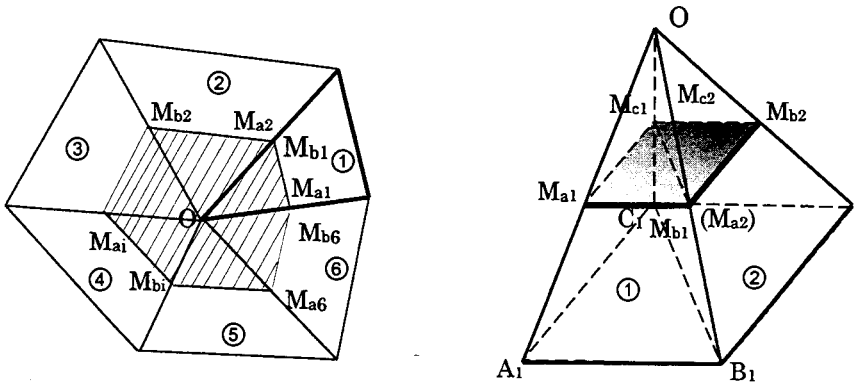

Fig.2. Construction of the primary and complementally cells. (a) Primary cells are triangles, and a shadowed region constructed by connecting the middle points of the edges is a complementally cell enclosing the common node O in 2D. (b) Primary cells are the tetrahedrons, and by connecting the middle section in each element which is opposite to common node O constructs the complementally cells enclosing the common node O in 3D. The shadowed region shows two middle sections parallel to the bottom surface in two adjacent elements with the common node O, respectively.

In 3D, primary cells are the tetrahedrons, and also one of the complementally cells is constructed in such the similar way as those of 2D. Shadowed surface in Fig.2(b) shows two of surfaces of one complementally cell around node O. In Fig.2(b), a node O is a common to the two adjacent primary cells ① and ②. In these primary cells ① and ②, M_{a1}, M_{b1}, M_{c1} are the middle points of the edges OA_1, OB_1 and OC_1 in tetrahedral elements ①, respectively. Thereby, a middle section M_{a1}-M_{b1}-M_{c1} is in parallel to the bottom surface $A_1B_1C_1$ of tetrahedral element ①. Similarly, a middle section M_{a2}-M_{b2}-M_{c2} is in parallel to the bottom surface of tetrahedral element ②. Hence, connecting all the middle sections of the tetrahedral elements enclosing the common node O leads to a complementally cell enclosing the node O. In each of the complementally cells, Eq.(5) reduces into a following discretized form as

$$\oint\!\!\!\oint_{S^{ith}} (-\sigma \nabla \varphi) \cdot d\bar{S}_i = 0 \tag{7}$$

where i refers to the i^{th} node in the primary cell as well as the i^{th} complementally cell, and S_i is the boundary of the i^{th} complementally cell enclosing the common i^{th} node.

Comparing to the other discretization with our methods reveals that the main advantages of our discretization method to generate the primary cell are as follows: 1) geometrical

singularity is removed, and 2) coefficient matrix is sparse and symmetrical [6].

3.2 Comparison between FVM and analytical solution

To verify the validity of FVM solution, we compare the FVM solution with analytical one for the 2D circular and 3D spherical models having homogenous media. Fig.3 shows the mesh systems for 2D and 3D FVM solutions.

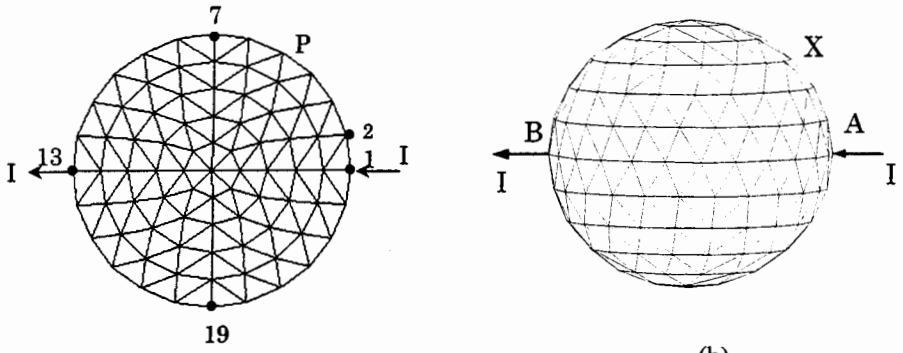

Fig.3. The mesh systems for 2D and 3D FVM solutions. (a) 2D circular model when injecting the current I through a pair of electrodes 1 and 13, where the primary cells have 81 nodes and 136 elements. (b) 3D unit spherical model when injecting the current I through a pair of electrodes A and B, where the primary cells have 184 nodes and 2469 elements.

The analytical solutions φ for 2D circular and 3D sphere with conductivity of σ are given by Eqs.(7) and (8), respectively, when injecting the current I through a pair of electrodes on the surface.

$$\varphi = \frac{I}{\pi\sigma} \ln \frac{R_2}{R_1} \tag{7}$$

where R_2 and R_1 are the distances from the observed point P to the driving electrodes 1 and 13, respectively[3].

$$\varphi = \frac{I}{4\pi\sigma}\left[\frac{2}{R_A} - \log\left(1 - \bar{X}\cdot\bar{A} + R_A\right)\right] - \frac{I}{4\pi\sigma}\left[\frac{2}{R_B} - \log\left(1 - \bar{X}\cdot\bar{B} + R_B\right)\right] \tag{8}$$

where R_A and R_B are the distances from the observed point X to the driving electrodes A and B, respectively. $\bar{X}$, $\bar{B}$ and $\bar{A}$ are the vectors from the center of sphere O to the points X, B and A, respectively[8].

Fig.4 shows the comparison between the analytical and FVM solutions. Observing the results in Fig.4 suggests that FVM gives a fairly good solution even though we employ a relatively coarse mesh system.

3.3 Numerical verification of methodology

With the construction of the object known, each subregion *i* has the constant conductivity of σ_i, then Eq.(3) can be discretized as:

$$\sum_{\Omega} \frac{1}{\sigma_i} \iiint_{\Omega_i} \mathbf{J}_1 \bullet \mathbf{J}_2 \, d\Omega_i = (\varphi_{1C} - \varphi_{1D}) \cdot I \tag{9}$$

To verify our conductivity derivation methodology based on the adjoint field theory when applying to the region having inhomogeneous conductivities, it is essentially required the current density distributions in Eq.(9). Thereby, at first, we compute potential distribution at the nodes with FVM, and then derive the current density distribution in each element based on the potential distribution by linear interpolation. By means of above processes, it is possible to simulate the current densities instead of MRI methodology. Thus, the potential on the surface can be obtained for simulation as well, and then by employing the Eq.(9), a system matrix can be constructed with the conductivities of subregions as the unknown parameters after carrying out the measurements as the same number as the subregions. By solving the inversion of the system matrix, the conductivity for each subregion can be obtained.

Fig.5(a) and 5(b) show the circular models having three layers and two different conductivities. Tables 1 and 2 list the computed values of conductivity together with that of exact one. In table 1, $\sigma 1, \sigma 2, \sigma 3$ are the exact conductivities of three layers solving for the forward EIT problem with FVM, $\hat{\sigma}1, \hat{\sigma}2, \hat{\sigma}3$ are the computed conductivities by our method. Similarly, $\sigma 1, \sigma 2$, are the exact conductivities and $\hat{\sigma}1, \hat{\sigma}2$ are the computed ones. Fig.6(a) and 6(b) shows the exact and computed results concerning to a circular model having 4 different conductivities, respectively. Table 3 lists the exact and computed values of conductivity. In table 3, O (x,y) denotes the x, y coordinate of the central position of small circular region having different conductivities to the others.

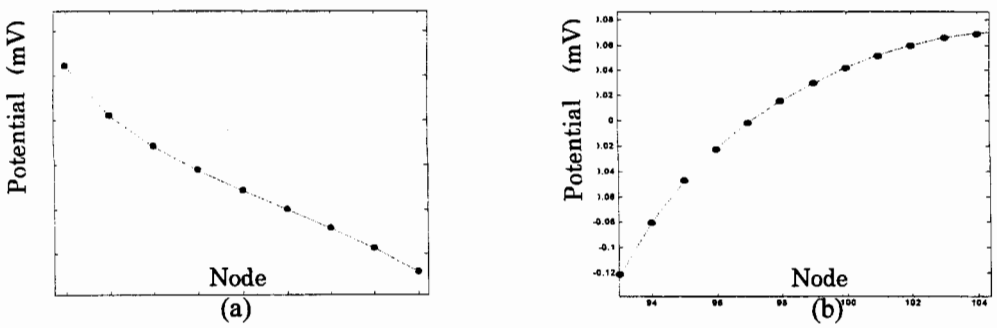

Fig.4. Comparison of analytical and FVM solutions. Solid and dotted lines show the analytical and FVM solutions, respectively. (a) 2D and (b) 3D.

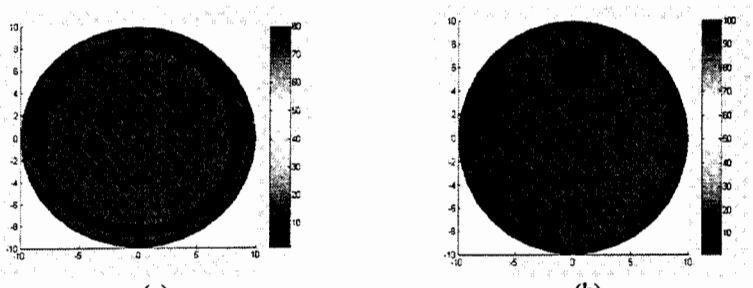

Fig.5. Circular models having (a) three layered and (b) two conductivities.

Table 1 Computed values of conductivity together with that of exact one.

	σ1	σ2	σ3	$\hat{\sigma}1$	$\hat{\sigma}2$	$\hat{\sigma}3$
1	10000	10	50	10000.0000	9.9999	50.0000
2	80	1	80	80.0000	0.9999	80.0000
3	100	50	20	99.9999	50.0000	19.9999
4	100	1	120	99.9999	1.0000	119.9999

Table 2 Computed values of conductivity together with that of exact one.

	O(x,y)	σ1	σ2	$\hat{\sigma}1$	$\hat{\sigma}2$
1	(6,0)	100	1	100.0000	0.9999
2	(4,4)	100	1	99.9999	1.0000
3	(-4,-2)	100	1	100.0000	0.9999
4	(0,6)	85	90	84.9999	89.9999

As for the 3D spherical model having different conductivities, we have carried out a lot of examinations. Fig.7 shows one of the spherical model having conductivities σ1, σ2, σ3, σ4. Table 4 lists the computed values of conductivity together with that of exact one.

From the results of both 2D and 3D, it is revealed that the absolute values of conductivities with high accuracy could be evaluated by our methodology based on the adjoint field theory, even though we employ a relatively coarse mesh system of FVM. This is because the numerical error accompanied with the computations of the original and adjoint fields may cancel each other.

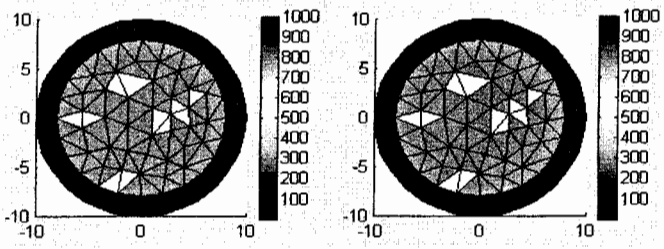

(a) (b)

Fig.6. (a) Exact conductivity distribution and (b) computed one.

Table 3 Computed values of conductivity together with that of exact one.

	Exact conductivities		Computed conductivities
σ1	100	$\hat{\sigma}1$	99.9999
σ2	1	$\hat{\sigma}2$	1.0000
σ3	120	$\hat{\sigma}3$	119.9999
σ4	50	$\hat{\sigma}4$	49.9999

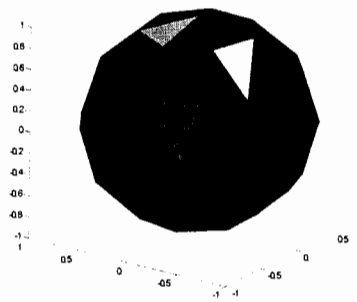

Fig. 7. 3D spherical model having four different conductivities. Major region has the conductivity of σ1, and the other small regions have the conductivities of σ2, σ3, σ4 and locate at the boundary.

Table 4 Computed values of conductivity together with that of exact one.

	Exact conductivities1	Exact conductivities 2		Computed conductivities 1	Computed conductivities 2
$\sigma 1$	10	40	$\hat{\sigma}1$	10.0000	40.0000
$\sigma 2$	110	112	$\hat{\sigma}2$	109.9999	112.0000
$\sigma 3$	210	220	$\hat{\sigma}3$	210.0000	219.9999
$\sigma 4$	310	71	$\hat{\sigma}4$	309.9999	71.0000

4 CONCLUSION

In this paper, we have applied our method based on the adjoint field theory to the 2D circular and 3D spherical regions having inhomogeneous conductivity distribution.

To verify our method in numerically, it has been essential to solve the EIT forward problem. We have employed FVM for solving this forward problem.

Intensive numerical simulations along with FVM have verified the validity of our new method.

Thus, we have established a new methodology based on the adjoint field theory to evaluate the absolute values of conductivity. It should be noted that cancellation between the original and adjoint field computational errors might lead to the estimation results with high accuracy.

5 REFERENCES

[1] Humberto R Gamba , D.T.Delpy, "Measurement of electrical current density distribution within the tissues of the head by magnetic resonance imaging", *Med. Biol. Eng. Comput*, 1998, 36, pp165-170

[2] Wang Xianchong, "Electric Magnetic Field Theory and Application." 1991, *Science Press*. China.

[3] Dong Guoya, Ma Xinshan, et al, "Derivation from Current Density Distribution to the Conductivity Based on Adjoint Field Theories and the Analytic Simulation Test", *ASAEM'2001*, Hangzhou, China.

[4] S.Abboud, Y.Eshel,et al , "Numerical clculation of the potential distribution due to dipole sources in a spherical model of the head", *Comp. Biomed. Res.*, Vol. 27, pp.441-455, 1994.

[5] Y.Eshel, S.Levy, "Correlation between skull thickness asymmetry and scalp potential estimated by a numerical model of the head", *IEEE Trans. Biomed. Eng.*, Vol. 42, pp. 242-249, 1995.

[6] Moshe Rosenfeld, Ronen Tanami, "Numerical solution of the potential due to dipole sources in volume conductors with arbitrary geometry and conductivity", *IEEE Trans. Biomed. Eng.*, Vol.43, No.7, pp.679-689, 1996.

[7] Luo Feilu, Wang Xianchong, "The generalized power of electric magnetic field and the method of weighted residuals of boundary problem", *Dian Gong Ji Shu Xue Bao*, 1985 (3)".

[8] A.Gibson, "Electrical Impedance Tomography of Human Brain Function", Department of Physiology, University College, London. July 2000, Ph.D Thesis.